ALPHA CLUSTER MODEL AND THE SPECTRUM OF ^{16}O

W. Bauhoff

I. Institut für Experimentalphysik, Universität Hamburg

D-2000 Hamburg 50, West Germany

and

School of Physics, University of Melbourne

Parkville, Victoria 3052, Australia*

and

H. Schultheis and R. Schultheis

Institut für Theoretische Physik, Universität Tübingen,

D-7400 Tübingen, West Germany

ABSTRACT

The structure of ^{16}O is studied in the alpha cluster model with parity and angular-momentum projection for several nucleon-nucleon interactions. The method differs from previous studies in that the states of positive and negative parity are determined without the customary restriction of the variational space to cluster positions with certain assumed symmetries. It turns out that a number of variational results in the literature are spurious under unrestricted variations. We demonstrate that the alpha cluster model of ^{16}O is capable of explaining most of the experimental T = 0 levels up to about 15 MeV excitation. In particular, the 6.05 MeV rotational band is reproduced remarkably well. A shell-model analysis of the excited cluster-model states

shows the necessity of including a very large number of shells. The evidence for the recently proposed tetrahedral symmetry of some excited states is also discussed.

NUCLEAR STRUCTURE. Alpha-cluster structure calculation without prescribed symmetry for B_1 and Skyrme III force for ^{16}O. Calculated T = 0 spectrum, densities, quadrupole moments, rms radii. Comparison with shell-model wave-functions.

PACS numbers: 21.10.Re, 21.60.Gx, 27.20.+n

I. INTRODUCTION

The properties of ^{16}O have been studied in a variety of approaches, including Hartree-Fock, shell-model and cluster-model calculations (for reviews see e.g. refs. [1-3]). Each method had only limited success in reproducing the experimental spectrum of ^{16}O over a satisfactory energy range without readjustment of the interaction. Especially the low-lying rotational band based on the 0_2^+ state at 6.05 MeV has a much higher calculated excitation energy in many cases. Shell-model calculations [4] which fit the experimental spectrum have problems with spurious contributions to the wave functions. Hartree-Fock (HF) studies predict a deformed excited state at about 15 to 30 MeV intrinsic excitation [5-9]. Projecting out states of definite angular momentum would probably reduce this energy considerably, because no energy is gained for the spherical ground state. No such calculation has yet been performed except in ref. [10] where, however, the excitation of excited states has been used to adjust the parameters of the force. Some calculations using cluster models [11-13] reproduce the experimental spectrum fairly well, but only by adopting different forces for different energy regions. Similar problems exist for the negative parity states. Only part of the low-lying levels have been obtained in shell-model [14] and RPA [15] calculations. Here, the rotational band based on the 1_2^- state at 9.63 MeV is particularly difficult to approximate.

These problems have motivated us to study the low-lying spectrum

of ^{16}O again. In doing so we will use Brink's alpha-cluster model (ACM) [16]. The model has sufficient flexibility to describe shell-model-like states (e.g. the ground state) and states with a well developed cluster structure (such as rotational bands). As intrinsic states without reflection symmetry are easily constructed in the ACM it also comprises negative-parity rotational bands, which in Hartree-Fock require particular modifications.

A number of calculations has been performed for ^{16}O using the ACM [17-25]. All of them, however, have restricted the model space by assuming *a priori* certain geometrical arrangements for the four alpha clusters, such as tetrahedrons, rhombs or chains. The energy is then minimized within this limited subspace only.This procedure may lead to erroneous results as we have previously shown [26-28] for sd-shell nuclei. It may turn out that the cluster positions of the true minimum-energy state and the usually assumed configurations have different point symmetries. We note here that a discrepancy exists for the ground state of ^{16}O, which is usually thought of as a regular tetrahedron, but has been claimed [23] to have a more elongated tetrahedral shape.

An alpha-cluster description of ^{16}O is of great interest for the problem of tetrahedral symmetry in light nuclei that has been discussed recently [29,30]. In the ACM angular-momentum eigenstates can be projected from intrinsic many-body states with tetrahedral symmetry. This can be compared with the previous assignment of group theoretically allowed states based

on a phenomenological adjustment of the parameters of a molecular Hamiltonian. If ^{16}O has a common intrinsic tetrahedral state for bands of positive and negative parity then the level scheme should differ from what is usually believed.

This paper has two parts. The first one deals with the intrinsic states obtained from unconstrained minimizations in the alpha-cluster space. We discuss the resulting local minima and compare with previous results that turn out to be unstable in many cases. In the second part we study the rotational bands of both positive and negative parity, that result from angular-momentum projection of the above intrinsic states, and compare the calculated bands with the experimental spectrum.

II. INTRINSIC STATES

A. The model

Brink's alpha cluster model has been discussed in detail in the literature [e.g. refs. 16,31] and we recall here only the basic definitions. The intrinsic variational many-body states Φ of the nucleus are constructed as Slater determinants of 1s harmonic-oscillator single-nucleon orbits centered around given cluster positions $\vec{R}_j$:

$$\phi_i(\vec{x}_i) = (b\sqrt{\pi})^{-3/2} \exp[-(\vec{x}_i - \vec{R}_j)^2/2b^2]\chi_i$$

$$(i = 1,\ldots,A;\ j = 1,\ldots,A/4). \qquad (1)$$

Here, i labels the nucleons and j the cluster centers, χ_i denotes the spin and isospin part of the wave function, and b is the

oscillator width. All states are occupied by four nucleons. A wave function of this type can describe states of shell-model character (all $\vec{R}_j$ are equal or close together) as well as states with a pronounced cluster structure where the positions $\vec{R}_j$ are well separated. This property makes the model well-suited for calculations in ^{16}O where both types of states exist. The assumption of fourfold occupation prevents, however, the description of particle-hole excitations other than 4p-4h, 8p-8h etc.

In general, this kind of many-body wave-function will neither be a parity nor an angular momentum eigenstate. So components with good quantum numbers have to be projected out of the intrinsic state. For the parity operator, this is achieved by using the linear combinations $|\Phi(\vec{R}_j)> \pm |\Phi(-\vec{R}_j)>$. In this model negative parity states can be described as easily as positive parity ones, provided that $|\Phi(\vec{R}_j)> \mp |\Phi(-\vec{R}_j)>$. The angular momentum projection is more involved and will be discussed in the next section.

The projection operators can be applied either before or after the variation of the parameters. For non-axial configurations the angular momentum projection involves a three dimensional integral that leads to large computing times. Therefore we project onto good angular momentum only after variation whereas the parity projection is always performed before variation. We note that this may lead to inaccuracies because a large energy gain has been found for a variation after projection of the ground state of ^{16}O [17]. This will be discussed below.

The variational parameters of the model are the cluster positions $\vec{R}_j$ and the oscillator width b. Usually the cluster positions are assumed to have certain geometrical properties that restrict the number of parameters. In contrast to that procedure we perform an unconstrained variation of all $3 \cdot 4 - 6 + 1 = 7$ variational parameters (here the 6 spurious rigid-body degrees of freedom are subtracted). Numerical searches for energy minima may give more than one of them. These correspond to the ground state and the excited intrinsic states on which rotational bands may be built. Finding minima different from the ground state turns out to be quite complicated. Energy minima have been determined numerically, starting at arbitrary points in the variational space. The iterative minimization usually leads to the ground state and only occasionally results in an excited local minimum which, if sufficiently deformed, may correspond to a rotational band. Actually such local minima are found only if the starting point is already close to the minimum. As a grid search is impractical in seven dimensions some uncertainty remains whether all minima have been located, even though a number of attempts to find additonal minima failed.

In order to see whether the results depend on the nuclear force in the Hamiltonian, we have used two different forces, the Brink-Boeker force B1 [32] and the Skyrme force SIII [33]. The two forces represent two rather different types. The B1 force has finite range and saturates through its odd state repulsion, the SIII force has range zero and is density dependent. In all cases the Coulomb interaction was included exactly and the

complete (one- and two-body) center-of-mass term has been taken into account. This eliminates problems with spurious states which occur in shell-model calculations [2].

B. Results for intrinsic states

In this subsection we discuss the results obtained for the intrinsic states. They are summarized in table I. For positive parity and for both forces the lowest energy state has cluster positions $\vec{R}_j$ that form a regular tetrahedron (see fig. 1a). We do not find that a deformed structure yields more binding as claimed in [23], where Coulomb effects have been neglected. Although the resulting distance between the centers is 1.27 fm for B1 and only 0.57 fm for SIII the calculated rms-radii differ by only 0.02 fm. The B1 energy is identical to the result of refs. [17-19,21], there is, however, a discrepancy in the radius. The results of HF calculations [6] are very similar in the B1 case. For SIII almost 8 MeV are missing in the binding energy. This shows that clustering is less favoured by SIII than by B1 in accordance with previous findings [20]. The radii are in good agreement with experiment, B1 underbinds considerably, as usual in this mass region, whereas SIII is close to the experimental binding energy.

Our results for excited intrinsic states differ more markedly both from previous ACM calculations and for the two forces. The first excited 0^+ state is usually assumed to consist of a planar rhomb configuration of the four clusters. In our unconstrained calculation it turns out that such a configuration is unstable

against bending about the shorter diagonal. Another instability which leads to a kite shape (see below) has been noted in ref. [22]. We find a stable configuration which is slightly non-planar (see fig. 1b) but maintains the overall shape of a rhomb. The gain in binding energy is almost 2 MeV (B1 force) as compared to the planar rhomb and also to the HF result. For the SIII force no state has been found with a rhomb-like configuration.

Since the shape parameters Q_o and Q_2 cannot be defined unambigously for such a triaxial state we have chosen the axes such that $|Q_2|$ is minimum and Q_2 is positive. All values refer to charge quadrupole moments. The experimental quadrupole moment of the excited state can be extracted from the measured γ-decay rate $\Gamma_\gamma = (2.7 \pm 0.3) \cdot 10^{-5}$ eV [34] for the transition 2^+(6.92 MeV) to 0^+(6.05 MeV). The formulas [37]

$$B(E2\downarrow) = 75/4\pi \cdot (\hbar c/E_\gamma)^5 \Gamma_\gamma \,, \tag{2}$$

$$B(E2\uparrow) = 5B(E2\downarrow) \tag{3}$$

and

$$B(E2\uparrow) = 5e^2/16\pi \cdot Q_o^2 \tag{4}$$

yield $Q_o = (58 \pm 4)$ fm^2 which is in good agreement with our result. However, the assumption of the rotational model in eq. (4) may not be well fulfilled in light nuclei. An earlier estimate [6] from experimental B(E2) values gives $Q_o = 64 \pm 4$ fm^2 and a HF calculation [7] $Q_o = 57$ fm^2 for the first excited 0^+ in ^{16}O.

A second excited state in the ACM is believed to have a square $\vec{R}_j$

configuration [17]. This shape also turns out to be unstable against bending about the diagonal. We find no stable state of a similar shape but a local minimum with a kite shape for both B1 and SIII (see fig. 1c). For B1 it is 4 MeV below the (spurious) square of minimum energy. The SIII excitation energy is almost twice as high as in the B1 case whereas the shape parameters are similar. We findno evidence for a different kite shape that has been studied in ref. [22]. Our kite is very close in energy and shape parameters to the bent rhomb. The configuration is quite interesting since three of the four alpha clusters form an almost equilateral triangle with a side length very close to the ground-state configuration of ^{12}C. In this sense the state has a $^{12}C + \alpha$ structure. Such a cluster model of ^{16}O has been proposed earlier [38], and there are resonating group calculations using a $^{12}C + \alpha$ partition [12]. Thus the ACM result provides a justification for this previously conjectured structure.

In the last positive parity excited state the clusters form a linear chain. In all previous calculations [17-19,22] the four clusters of the chain have been arranged symmetrically with two or three equal distances. Thus only intrinsic states with positive parity have been considered. In contrast to this we find for both forces that the stable solution has three different distances (see fig. 1d). We emphasize that the linear arrangement and the stability against bending is a result rather than a constraint of our variation. For B1 the gain in binding energy over the symmetric configurations [17-19,22] is more than 1 MeV. Again, SIII gives about twice the excitation energy of B1 but

only marginally different shape parameters.

For negative parities two local minima have been found. The lower configuration is a regular tetrahedron with separations between the clusters that are almost twice as large as for positive parity: 2.59 fm for B1 and 1.04 fm for SIII. We therefore consider this state as an octupole vibration of the ground state, corresponding to the lowest 3^- state (cf. sect. III). The SIII force has higher excitation energy than B1 but a similar rms radius.

Previous constrained ACM calculations [17,22] have led to a tetrahedral configuration with negative parity. In addition to that we find a second local minimum with negative parity. The configuration has a kite shape (see fig. 1e) different from the kite-shaped positive-parity minimum. It also differs from the one assumed in ref. [22] which seems to be unstable. The size of the triangular substructure is larger than for positive parity and very close to the lowest configuration of negative parity in ^{12}C. Thus both intrinsic "kite" states in ^{16}O are consistent with an $\alpha + {}^{12}C$ structure. For SIII we find again a higher excitation energy and a somewhat smaller deformation than for B1. Hartree-Fock results with negative parity are not available for comparison.

Summarizing the differences between B1 and SIII, we note that, because of the much higher excitation energies in the latter case, it is unlikely that the projected energies can be close to the experimental levels. This is not peculiar to the ACM but has

also been observed in HF calculations [10]. In the next section we will therefore consider only the B1 results. The shape parameters are similar for the two forces with SIII leading to somewhat smaller deformations. The degree of clustering can be seen better from density contour plots which will be discussed below.

In order to study the discrepancies between our results and previously published values for the intrinsic configurations we restrict the variational space by parametrizing the cluster positions in the following way:

$$\vec{R}_1 = (d_1, 0, -d) \tag{5a}$$

$$\vec{R}_2 = (-d_1, 0, -d) \tag{5b}$$

$$\vec{R}_3 = (0, d_2, d) \tag{5c}$$

$$\vec{R}_4 = (0, -d_2, d) \ . \tag{5d}$$

This corresponds to two orthogonal dumbbells that are $2d_1$ and $2d_2$ long and separated by a distance of 2d. Most of the configurations considered in the ACM can be parametrized in this way: tetrahedron ($d_1 = d_2 = \sqrt{2}d$), planar rhomb ($d_1 \neq d_2$, $d = 0$) and square ($d_1 = d_2$, $d = 0$). A bent rhomb is given by $d_1 \neq d_2$ and $d \neq 0$. The shell-model ground state is obtained for $d_1 = d_2 = d = 0$.

For each value of d, we have minimized the energy with respect to d_1, d_2, and the cluster size b. The results are shown in fig. 2 for positive ($P = +1$) and negative ($P = -1$) parity and for a calculation without parity projection ($P = 0$). For all values of d, a symmetric minimum exists with $d_1 = d_2$. This curve contains

the tetrahedral ground state which lies at finite d for P = +1 and P = -1. For P = 0, however, the minimum is obtained for d = 0, and corresponds to the shell-model ground state. A second and third minimum occurs at small values of d except for negative parity. The second one has an asymmetric shape ($d_1 \mp d_2$) and goes over into the rhomb for d = 0. This configuration is a saddle point in the restricted space. At finite d a local minimum is obtained only for P = +1 which is the bent rhomb described above. The existence of this state depends on whether the parity projection is performed before or after variation. A similar observation has been made in a HF calculation [39]. The third minimum finally goes over into a square for d = 0 which is again only a saddle point. No minimum is found, however, for finite d in this case. Therefore the previous variation of a square-shaped ACM state has led to a spurious result.

The low symmetry of some intrinsic configurations (bent rhomb, chain with three different separations) may be surprising. An explanation for this is given in fig. 1 where the parity-reflected configuration is shown in dashed lines. Here the combined density of solid and dashed circles together corresponds to clusters with prolate deformation. The resulting cluster configurations would be more symmetric if the clusters were allowed to deform. This explanation would also apply to the chain structure in ^{12}C that has been found to be unstable against bending except for a finite hinge angle [40].

The prolate deformation can also be seen in the contour plot (fig. 3) for the density of the chain after projection onto

positive parity. Figure 4 shows the density of the kite configuration in the plane of the kite. Because of the parity projection the characteristic $^{12}C + \alpha$ distribution of fig. 1c is not visible here. It is apparent from the plot that the cluster structure is more pronounced for B1 than for SIII. Generally the odd-state repulsion of B1 tends to favour clustering as already noted earlier [20].

C. Comparison with Shell-Model Wave Functions

For vanishing cluster separation the ACM wave function goes over into a shell-model wave function. The tetrahedron, e.g., approaches the ground-state configuration $(1s)^4 (1p)^{12}$ in the limit of vanishing side-length [16]. For finite separation such a one-to-one correspondence does not exist. We have therefore studied an expansion of the ACM wave function in terms of shell-model states. Such an expansion will be of some interest because of the failure of the shell model to describe the low-lying rotational bands.

The number of possible shell-model states increases very rapidly with the number of shells. In order to have a manageable set we consider only one kind of particles (e.g. neutrons with spin-up). This still requires 10^6 states for the non-planar configurations. The number is greatly reduced for planar or linear configurations because then only 1s orbits contribute in one or two directions.

The results are shown in fig. 5. The probabilities for the positive parity ACM configurations are plotted versus the number

of oscillator quanta in the shell-model wave function. Here $0\hbar\omega$ denotes the shell-model state with no particle-hole excitation. The $2\hbar\omega$ terms include both the excitation of one particle by two major shells and the simultaneous excitation of two particles by one shell each. The states with more oscillator quanta are constructed in the same way. Because here only one particle of each ($T = 0$, $S = 0$) quartett is considered the label $1\hbar\omega$ actually refers already to a 4p - 4h excitation.

The probability for the tetrahedron is seen to be concentrated at $0\hbar\omega$: The ACM configuration does not deviate very much from the simple shell-model ground state. For all other states the probability is spread out over many shells. Therefore a shell-model calculation in a basis which is large enough to cover an adequate portion of the ACM wave function will be impractical. Earlier $^{12}C + \alpha$ orthogonality-condition model studies had similar results [11]. The lowest excited state e.g. is assumed to be of 4p - 4h type in the shell model. The corresponding rhomb configuration has, however, only 29% overlap with this state, and in order to exhaust 90% of the ACM state the inclusion of $5\hbar\omega$ would be necessary. The situation is even worse for the chain which is treated as an 8p - 8h state in the shell model. The ACM chain has almost no overlap with this state. The shell model fails for these states because the number of shells taken into account is much too small. However, a significant increase in this number is beyond present computing capabilities.

A marked difference exists between the results for B1 and SIII. In the latter case the number of oscillator quanta needed is much smaller: The ACM states are much more shell-model like. We have

found in the last subsection that the excitation energies are much higher for SIII. These two facts may be related such that a low excitation energy is found only for states which deviate strongly from the shell-model form.

III. ANGULAR MOMENTUM PROJECTION AND SPECTRA

A. Point Symmetry and K-Selection Rules

As pointed out already in section II.A the ACM many-body wave functions are in general not eigenfunctions of the angular momentum operator. So it is necessary to project out states of good angular momentum by using the Peierls-Yoccoz projection operator

$$P^J_{KM}|\phi(\vec{R}_j)\rangle = \frac{2J+1}{8\pi^2}\int_0^\pi d\beta \sin\beta\, d^J_{KM}(\beta)\int_0^{2\pi} d\alpha \int_0^{2\pi} d\gamma\, e^{i(M\alpha + K\gamma)}$$

$$|\phi(R_3(\alpha)R_2(\beta)R_3(\gamma)\vec{R}_j)\rangle . \qquad (6)$$

Spectra are then calculated as expectation values of the Hamiltonian with these projected states. The threefold integration over the Euler angles has to be performed numerically. Though the necessary computing time can be reduced by a judicious choice of the meshpoints [31], it is still too large for projections before variation. Only for axial states, such as the chain, the integral reduces to a one-dimensional one which is much easier to handle.

The possible K-bands and corresponding J values can be determined by group-theoretical methods without performing the integration [16]. If the intrinsic state is invariant under a finite group

of rotations S with g elements then the number of states with a given angular momentum J is not greater than

$$N_J = \frac{1}{g} \sum_{S \epsilon S} \chi^J(S) \qquad (7)$$

where the sum runs over all group elements and $\chi^J(S)$ denotes the corresponding character.

If the symmetry group is not too large simpler formulas can be given :

(i) For axial symmetry, only K = 0 is possible with the states 0^+, 2^+, 4^+,.. or 1^-, 3^-, 5^-,... This applies to the chain.

(ii) For an axis of n-fold symmetry K may be 0, $\pm$ n, $\pm$2n,... For K = 0 we have again the states of (i), whereas for K $\neq$ 0 the possible states are |K|, |K| + 1, |K| + 2,... for positive and negative parity. This applies to the bent rhomb and to the kite with n = 2.

The tetrahedron is more difficult because of the large symmetry T_d. The above formula and the character table for T_d [41] lead to the following possible states: 0^+, 3^-, 4^+, 6^+, 7^-, 8^+,... Different K-values are degenerate in this case.

B. Tetrahedral Symmetry in ^{16}O

For B1 we have studied the positive and negative parity states with intrinsic tetrahedral symmetry because of Robson's recent investigations [29,30] of such a symmetry in light nuclei. In this work the rotational states of the tetrahedron are identified with the experimental levels 3^- (6.13), 4^+ (10.35) and 6^+ (16.29 MeV).

Using the Hamiltonian for tetrahedral molecules [42] with the parameters fixed by these three states, a 7^- and an 8^+ level are then predicted at 21.19 MeV and 29.18 MeV, respectively. This level assignment is completely different from the conventional one.

Positive and negative parity states are obtained from the same intrinsic state in refs. [29,30]. Our sol tions for plus - and minus parity turn out to have different intrinsic states. If one performs the variation before parity projection to maintain a common intrinsic (P = 0) state, the tetrahedron collapses (see fig. 2) to a point and this solution has $J^\pi = 0^+$ only. The variation after (P = +1)-projection leads to a tetrahedron with a side length of 1.27 fm (solution I), the (P = -1) result is 2.59 fm (solution II). The angular momentum projection of solution I gives the 3^- level at 13.26 MeV, 4^+ at 25.45, 6^+ at 26.87, 7^- at 38.55, and 8^+ at 50.25 MeV. For the corresponding projections of solution II we find these levels at 12.52, 22.58, 26.11, 35.75 and 46.22 MeV, respectively. All these excitation energies refer to the 0^+ ground state of the particular solution (I or II). The energies are considerably higher than those obtained in ref. [29]. They are lower for solution II which has a larger separation of the clusters. The energies are lower for a bigger tetrahedron but then the charge radius becomes too large.

We have also used our calculated energies of the 3^-, 4^+ and 6^+ states to determine the parameters B, D_s, and D_t of the Hamiltonian for tetrahedral molecules [42]

$$H = B\,J(J+1) - D_s[J(J+1)]^2 - D_t\,\langle O_{pppp}\rangle \qquad (8)$$

(the numbers $\langle O_{pppp}\rangle$ are given explicitely in [42]). An extrapolation of the $J^\pi = 7^-$ and 8^+ energies in the same way as in ref. [29] gives then 43.57 MeV and 87.40 MeV for solution I and 37.22 MeV and 65.07 MeV for solution II. These values for the molecular Hamiltonian differ from the energies obtained from angular momentum projection by up to 37 MeV. It should be noted that eq. (8) accounts for interaction terms up to the 4th order. Obviously with increasing angular momenta (such as 8^+) the higher order terms in the interaction become important, and may lead to large deviations from the exact angular momentum projection.

It is conceivable that the full variations after projection onto 3^-, 4^+, 6^+, 7^- and 8^+ would lead to ACM results that are closer to that of ref. [29]. However, the ACM results obtained so far (parity projection before and angular momentum projection after variation) do not agree with the concept of a molecular motion with tetrahedral symmetry, even though the intrinsic ACM ground state is a regular tetrahedron.

C. States of Positive Parity

In this subsection we discuss all positve parity bands that can be projected from intrinsic minimum-energy states. In addition to the tetrahedral states mentioned above there are K = 0 and K = 2 rotational bands for both bent rhomb and kite shape, and a K = 0 rotational band for the chain. All levels up to J = 10

and 30 MeV excitation energy are shown in fig. 6 together with the negative parity states that will be discussed in the next section.

Since the energies of a rigid rotor are

$$E_{JK} = \frac{\hbar^2}{2\theta_1} [J(J+1) - K^2] + \frac{\hbar^2}{2\theta_3} K^2 \qquad (9)$$

the level spacings of such rotational bands follow certain rules that can be checked easily without knowing the moment of inertia.

The spacing within a band with definite K-value is given by

$$[E_{JK} - E_{KK}]/[J(J+1) - K(K+1)] = \frac{\hbar^2}{2\theta_1} = \alpha = \text{const.} \qquad (10)$$

From

$$[E_{JK} - E_{JO}]/K^2 = \frac{\hbar^2}{2\theta_3} - \frac{\hbar^2}{2\theta_1} = \beta = \text{const} \qquad (11)$$

follows that all K bands with the same intrinsic state are parallel. High K values lie much higher in energy because $E_{J4} - E_{JO} = 4 \cdot (E_{J2} - E_{JO})$ for $J \geq 4$. Therefore, K = 4 and higher bands have not been calculated. We also do not take into account a possible mixing between K = 0 and K = 2 bands.

The calculated rotational bands show rather diverse patterns as compared to the rigid rotor. Kite and chain give rise to bands very close to the rigid-rotor case. For the kite we find rotational constants, averaged over the band members, of α = 192 keV for K = 0 and α = 188 keV for K = 2. The spacing between the K = 2 and K = 0 levels yields β = 257 keV. These values are close to

the classical moment of inertia of the corresponding arrangement of four α-particles. For the chain we find $\alpha = 64$ keV for the angular momentum projection in exact agreement with the classical calculation (β is not defined in this case). On the other hand, the bent rhomb is not a good rotor. The K = 0 band does not follow a J(J + 1)-spacing. The K = 2 band differs even from the normal level ordering of increasing energy with increasing angular momentum: The 7^+ state lies above the 8^+ state. Such an inversion has been found previously [43]. Although angular momentum projection must not lead to the normal level ordering such a deviation may indicate that the intrinsic minimum energy state depends on the angular momentum and should be projected before variation. Still it is remarkable that similar configurations such as rhomb and kite show such a different behaviour in their rotational spectrum. The extraction of α and β does not seem meaningful in this case. The same is true for the tetrahedron.

We turn now to a comparison of the calculated spectrum with the experimental levels [34]. In fig. 7 we have plotted the excitation energy versus J(J + 1) to facilitate the identification of rotational bands. All experimental states with positive or unknown parity and zero or unknown isospin have been included. States with uncertain J^π assignment are in brackets. No 5^+ or 7^+ states are known experimentally, and only one 8^+.

Only two positive-parity rotational bands are well established. The first one is the low-lying band based on the 0^+(6.05 MeV) state which is known at least up to 6^+(16.28 MeV) and up to

8^+(22.5 MeV) with some uncertainty. The other band is the high-lying band associated with a linear configuration of four α-clusters whose band head (0^+) has not been observed. In fig. 7 we have indicated some more level sequences that possibly form rotational bands. The band assignment relies mainly on the J(J+1)-spacing of the levels. This envolves, of course, some ambiguity. In fact, some bands have been assigned differently in ref. [44], a search based on the experimental spectrum, and in ref. [45], an attempt to use an eight-particle liquid-drop plus shell-correction approach with large readjustments for the band heads. The band assignments of fig. 7 follow partly earlier proposals [46]. We find a K = 2 band based on the 2^+(9.85 MeV), an additional K = 0 band based on the 0^+(11.25 MeV) and a corresponding K = 2 band starting at 2^+(15.26 MeV). All these bands can be traced up to 6^+ with the 5^+ states missing in the K = 2 bands. No additional rotational band can be identified with a band head below 15 MeV. So altogether we have three K = 0 and two K = 2 bands.

This number coincides with the number of rotational bands resulting from our calculation. Therefore, a one-to-one correspondence can be established. The identification is rather unambigous for the band associated with the chain. We obtain the band head at 16.27 MeV and a rotational constant of 64 keV in very close agreement with refs. [17-19] and experimental data (16.75 MeV and 63 keV, respectively). The lowest band at 6.05 MeV compares well with the one obtained from the rhomb. The calculated band starts at 5.45 MeV and the 8^+ is found at 23.43 MeV instead of

the experimental 22.5 MeV. Thus the calculated level positions reproduce the experimental values, in particular the band head, with an accuracy that is extraordinary for a microscopic calculation with a standard nucleon-nucleon interaction and without adjustable parameters.

The calculated K = 2 band has large deviations from the J(J+1)-spacing as noted above, and such a behaviour is not seen experimentally. Also the calculated spacing between K = 0 and K = 2 states of fixed J^{π} is much too small.

We identify the remaining band, with the kite-shaped intrinsic state, with the 11.25 MeV band. It is about 4 MeV to low in energy but the rotational constant α = 192 keV is reasonably close to that deduced from the experimental spacing (about 200 keV). This time the difference between K = 0 and K = 2 is larger than for the rhomb, but still too small. The calculation yields 0.90 MeV rather than 2.24 MeV for the 2^+ state. The 4^+ and 6^+ states projected from the tetrahedron lie too high to be unambiguously identified with experimental levels.

Not all experimental positive-parity levels of ^{16}O can be classified in terms of rotational bands. Some are possible candidates for vibrational states.

The states $(0^+,2^+,4^+)$ around 11 MeV have been proposed as candidates for a two-phonon triplet [46]. A recent $2\hbar\omega$ shell-model calculation [47] suggests a 2p-2h character for these states. Both explanations lie outside the scope of the present paper. The calculation of vibrational states requires the treatment of the cluster position as generator coordinates, and for 2p-2h states the quartett symmetry has to be broken.

D. States of Negative Parity

The number of negative parity states obtained in the ACM is much smaller than that for positive parity. Only two rotational bands are found, associated with the kite-shaped intrinsic state, and some states projected from the tetrahedron. The only tetrahedral state that can be identified in the experimental spectrum is the 3^- state at 6.13 MeV for which the calculation yields 4.86 MeV. The 7^- is too high to be assigned to a specific experimental level. As for positive parity the kite gives rise to a rotational band which is close to the rigid rotor form. The rotational constants are α = 141 keV for K = 0 and α = 140 keV for K = 2 and β = 331 keV, deduced from the angular momentum projection. This is in close agreement with the α-value for the classical moment of inertia.

Experimentally a $K = 0^-$ band is well established with the members 1^-(9.63), 3^-(11.60), 5^-(14.66), and 7^-(20.86 MeV). The position of the band head is close to the calculated one whereas

the experimental slope of the band is larger than calculated α_{exp} = 195 keV.

A possible $K^{\pi} = 2^-$ band can be constructed from the states 2^- (12.53), 3^-(14.1), and 5^-(18.40 MeV). A 4^- state in this energy range is not known. The known 4^- states [48] between 18 and 20 MeV are 1p - 1h excitations of stretched type $(1d_{5/2}, 1p_{3/2}^{-1})$, and do not belong to rotational bands. In comparison to the calculation the above candidate for a K = 2 band has a larger slope than for K = 0 and a larger spacing between the K = 2 and K = 0 bands. For 3^-, the calculation yields 1.34 MeV rather than 2.50 MeV, similar to the finding for positive parity.

Most of the low-lying negative parity states are considered as 1p - 1h excitations from the p- to the (sd)-shell. States of this type are outside the cluster model space. Some of the low-lying states are, however, not explained in a $1\hbar\omega$ shell-model calculation [2]. These are just the above candidates that can be described by the cluster model.

IV. CONCLUSION

In this paper we have considered in detail the ACM for ^{16}O. The treatment differs from previous studies in that it is based on an unconstrained variation of all seven parameters. Apart from this several of the usual approximations have been used. An angular momentum projection before variation was beyond our computing facilities. Mixing between different K-values and different intrinsic states (which are not necessarily orthogonal)

has not been considered. The existence of deformed α-clusters is suggested by some of the resulting intrinsic states, but has not been explored in detail.

A number of configurations obtained previously in restricted ACM variations turn out to be spurious. They are found unstable against certain variations and thus do not represent local minima of the energy surface. We have determined four local minima for positive parity and two for negative parity. The angular momentum eigenstates projected from these can explain most of the low-lying levels of ^{16}O. States not obtained within our model can be attributed to excitation mechanisms that lead out of our model space. Especially, we find in a parameter-free way a rotational band close to the well-known experimental 6.05 MeV band which shell-model calculations failed to describe. The analysis of our intrinsic state in terms of shell-model states shows the necessity of including a prohibitively large number of shells in such calculations.

The recent suggestion that the ^{16}O spectrum may be described in terms of a common intrinsic molecular state with tetrahedral symmetry is not supported by our results. While the tetrahedral symmetry of the ground state is confirmed the size of excited tetrahedral intrinsic states turns out to be different for positive and negative parity.

The authors acknowledge helpful discussions with Prof. K. Wildermuth. This work was supported in part by the Deutsche Forschungsgemeinschaft and by the Australian Research Grant Scheme.

REFERENCES

* present address

[1] J.P. Svenne, in Advances in Nuclear Physics, edited by J.W. Negele and E. Vogt (Plenum, New York, 1979), Vol. 11, p. 179.

[2] J.M. Irvine, C.D. Latorre and V.F.E. Pucknell, Adv. in Phys. 20, 661 (1971).

[3] Y. Fujiwara et al., Suppl.Progr.Theor.Phys. 68, 29 (1980).

[4] A.P. Zuker, B. Buck and J.B. McGrory, Phys.Rev.Lett. 21, 39 (1968).

[5] S.J. Krieger, Phys.Rev.Lett. 22, 97 (1969).

[6] J. Zofka and G. Ripka, Nucl.Phys. A168, 65 (1971).

[7] H.C. Lee and R.Y. Cusson, Ann.Phys. 72, 353 (1972).

[8] K.R. Lassey, M.R.P. Manning and A.B. Volkov, Can.J.Phys. 51, 2522 (1973).

[9] N.E. Reid, N.E. Davison and J.P. Svenne, Phys.Rev. C9, 1882 (1974).

[10] E. Caurier and B. Grammaticos, Nucl.Phys. A279, 333 (1977).

[11] Y. Suzuki, Progr.Theor.Phys. 55, 1751 (1976).

[12] Y. Suzuki, Progr.Theor.Phys. 56, 111 (1976).

[13] Y. Suzuki, T. Ando and B. Imanishi, Nucl.Phys. A295, 365 (1978).

[14] J.P. Elliott and B.H. Flowers, Proc.Royal Soc. A242, 57 (1957).

[15] V. Gillet and N. Vinh Mau, Nucl.Phys. 54, 321 (1964).

[16] D.M. Brink, in Many-Body Description of Nuclear Structure and Reactions, International School of Physics "Enrico Fermi", Course XXXVI, ed. by C. Bloch (Academic, New York, 1966), p. 247.

[17] D.M. Brink, H. Friedrich, A. Weiguny and C.W. Wong, Phys. Lett. 33B, 143 (1970).

[18] H. Friedrich, diploma thesis (University, Freiburg, 1971) unpublished.

[19] H. Friedrich and A. Weiguny, Phys.Lett. 35B, 105 (1971).

[20] S.B. Khadkikar, Phys.Lett. 36B, 451 (1971).

[21] K. Ananthanarayanan, S. Das Gupta and N. De Takacsy, Phys. Lett. 37B, 143 (1971).

[22] H. Friedrich, H. Hüsken and A. Weiguny, Phys.Lett. 38B, 199 (1972).

[23] C. Abulaffio and J.M. Irvine, Phys.Lett. 38B, 492 (1972).

[24] Y. Abgrall and E. Caurier, J.Physique 32, C6-63 (1971).

[25] C. Bargholtz, Nucl.Phys. A243, 449 (1975).

[26] W. Bauhoff, H. Schultheis and R. Schultheis, Phys.Lett. 95B, 5 (1980).

[27] W. Bauhoff, H. Schultheis and R. Schultheis, Phys.Lett. 106B, 280 (1980).

[28] W. Bauhoff, H. Schultheis and R. Schultheis, Phys.Rev. C26, 1725 (1982).

[29] D. Robson, Phys.Rev.Lett. 42, 876 (1979).

[30] D. Robson, Phys.Rev. C25, 1108 (1982).

[31] A. Arima, H. Horiuchi, K. Kubodera and N. Takigawa, in Advances in Nuclear Physics, ed. by M. Baranger and E. Vogt (Plenum, New York, 1972), Vol.5, p. 345.

[32] D.M. Brink and E. Boeker, Nucl.Phys. A91, 1 (1967).

[33] M. Beiner, H. Flocard, N.V. Giai and P. Quentin, Nucl. Phys. A238, 29 (1975).

[34] F. Ajzenberg-Selove, Nucl.Phys. A375, 1 (1982).

[35] J.H.E. Mattauch, W. Thiele and A.H. Wapstra, Nucl.Phys. 67, 1 (1965).

[36] R. Hofstadter, Nuclear and Nucleon Structure (W.A. Benjamin, New York, 1963) p. 392.

[37] K.E.G. Löbner, in Proceedings on the Electromagnetic Interaction in Nuclear Spectroscopy (North Holland, 1975)p. 141.

[38] R.K. Sheline and K. Wildermuth, Nucl.Phys. 21, 196 (1960).

[39] G. Do Dang, K.W. Schmid, R.M. Dreizler and H.G. Miller, Phys.Lett. 62B, 1 (1976).

[40] H. Friedrich, L. Satpathy and A. Weiguny, Phys.Lett. 36B, 189 (1971).

[41] H. Watanabe, Operator methods in ligand field theory (Prentice-Hall, Englewood Cliffs, 1966).

[42] K.T. Hecht, J. Mol. Spect. 5, 355 (1960).

[43] H.A. Lamme and E. Boeker, Nucl.Phys. A136, 609 (1969).

[44] H. Schultheis and R. Schultheis, Phys.Rev. C27, 1367 (1983).

[45] S. Åberg, I. Ragnarsson, T. Bengtsson and R.K. Sheline, Nucl.Phys. A391, 327 (1982).

[46] I. Ragnarsson, S.G. Nilsson and R.K. Sheline, Phys.Rep. 45, 1 (1978).

[47] K. Amos et al., Nucl.Phys., to be published.

[48] R.S. Henderson et al., Aust.J.Phys. 32, 411 (1979).

TABLE CAPTION

Table I: Energies E, root mean-square radii r, and charge moments Q_o and Q_2 for the intrinsic states of positive (P=+1) and negative (P=-1) parity. The excitation enegies are relative to the ground-state energy for the same force as given in the upper part.

Table I

configuration	P	method	force	E(MeV)	r(fm)	Q_o(fm^2)	Q_2(fm^2)	Ref.
tetrahedron	+1	ACM	B1	-94.4	2.68	0.	0.	this work
tetrahedron	+1	ACM	B1	-94.4	2.62	0.	0.	[17-19,22]
(000) (001) (010) (100)	+1	HF	B1	-93.0	2.65	0.	0.	[6]
tetrahedron	+1	ACM	SIII	-120.5	2.66	0.	0.	this work
(000) (001) (010) (100)	+1	HF	SIII	-128.2	2.69	0.	0.	[33]
		exptl.		-127.6	2.64-2.73	0.	0.	[34-36]
bent rhomb	+1	ACM	B1	15.2	3.16	67.0	10.7	this work
planar rhomb	+1	ACM	B1	17.1				[17,18]
kite	+1	ACM	B1	15.7				[22]
(000) (001) (010) (002)	+1	HF	B1	17.8	3.09	60.4	12.0	[6]
kite	+1	ACM	B1	16.2	3.22	76.0	11.4	this work
square	+1	ACM	B1	20.5				[17,18]
kite	+1	ACM	SIII	32.8	3.11	61.3	6.7	this work

Table I, continuation

asymm.chain	+1	ACM	B1	23.5	4.80	313.	0.	this work
symm. chain	+1	ACM	B1	24.8	4.62	290.	0.	[18,19]
equidist.chain	+1	ACM	B1	24.8				[17,22]
asymm.chain	+1	ACM	SIII	49.0	4.50	257.	0.	this work
tetrahedron	-1	ACM	B1	8.1	2.76	0.	0.	this work
tetrahedron	-1	ACM	B1	8.1				[17,22]
tetrahedron	-1	ACM	SIII	13.4	2.73	0.	0.	this work
kite	-1	ACM	B1	20.7	3.61	115.	12.5	this work
kite	-1	ACM	B1	22.5				[22]
kite	-1	ACM	SIII	37.0	3.28	78.9	6.5	this work

FIGURE CAPTIONS

Fig. 1: The various configurations found in the unconstrained variation. The parity reflected configuration is shown in dashed lines. The sizes are arbitrary.

a) tetrahedron

b) bent rhomb

c) kite (positive parity)

d) chain

e) kite (negative parity)

Fig. 2: Energy of the two-dumbbell configuration as a function of the separation for positive (dashed line), negative (dotted line) and no parity (solid line) projection.

Fig. 3: Density contour plot for the chain configuration for the B1 force. The contours are plotted in steps of 10% of the peak density.

Fig. 4: Density contour plot for the kite configuration for B1 (left) and SIII force (right).

Fig. 5: Probability to find various shell-model states in the ACM configuration.

Fig. 6: Calculated levels for positive and negative parity.

Fig. 7: Experimentally known levels in ^{16}O with positive or unknown parity and iso-spin zero or unknown. For points in parantheses the spin is uncertain. The band assignments are discussed in the text.

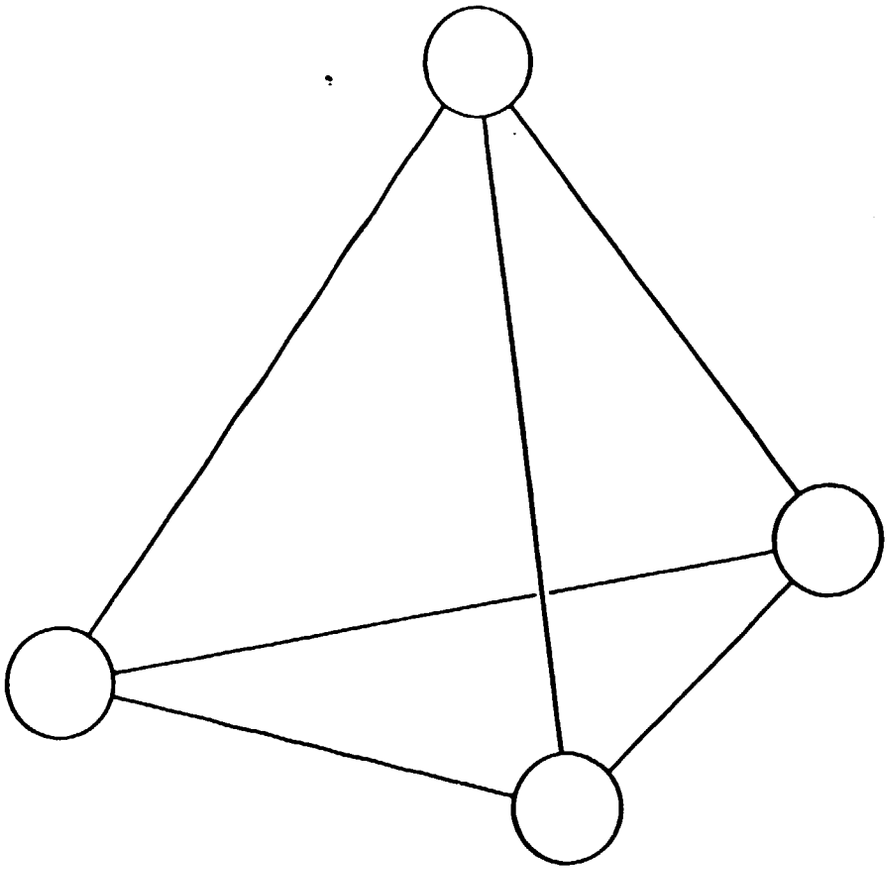

Fig. 1a

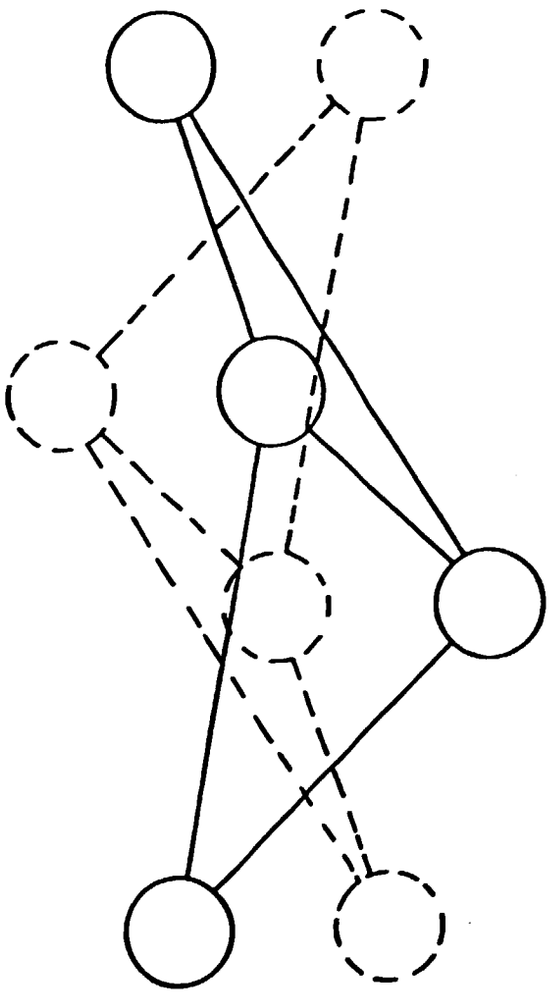

Fig. 1b

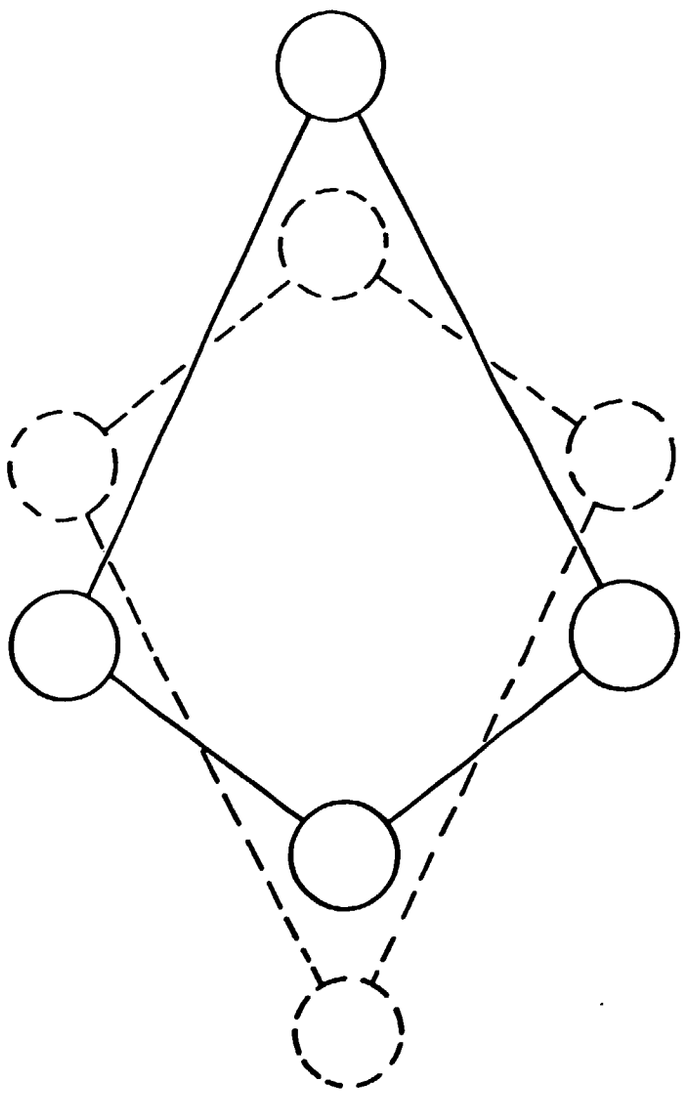

Fig. 1c

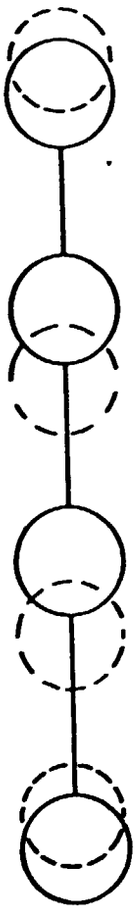

Fig. 1d

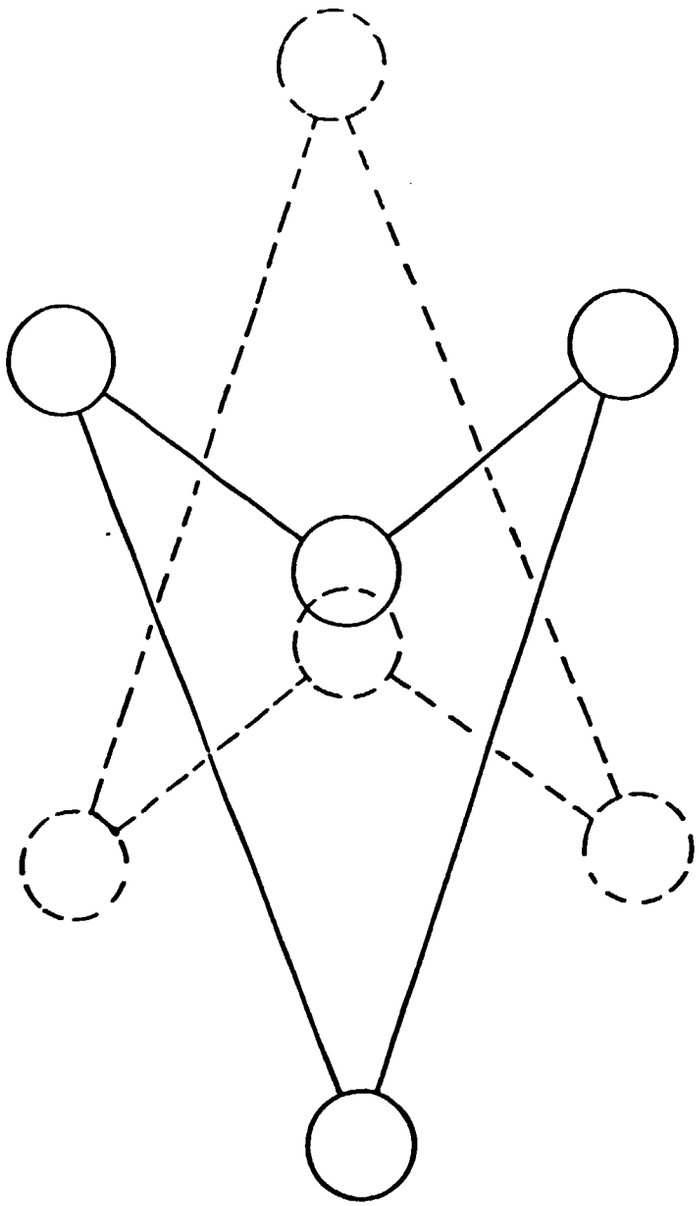

Fig. 1e

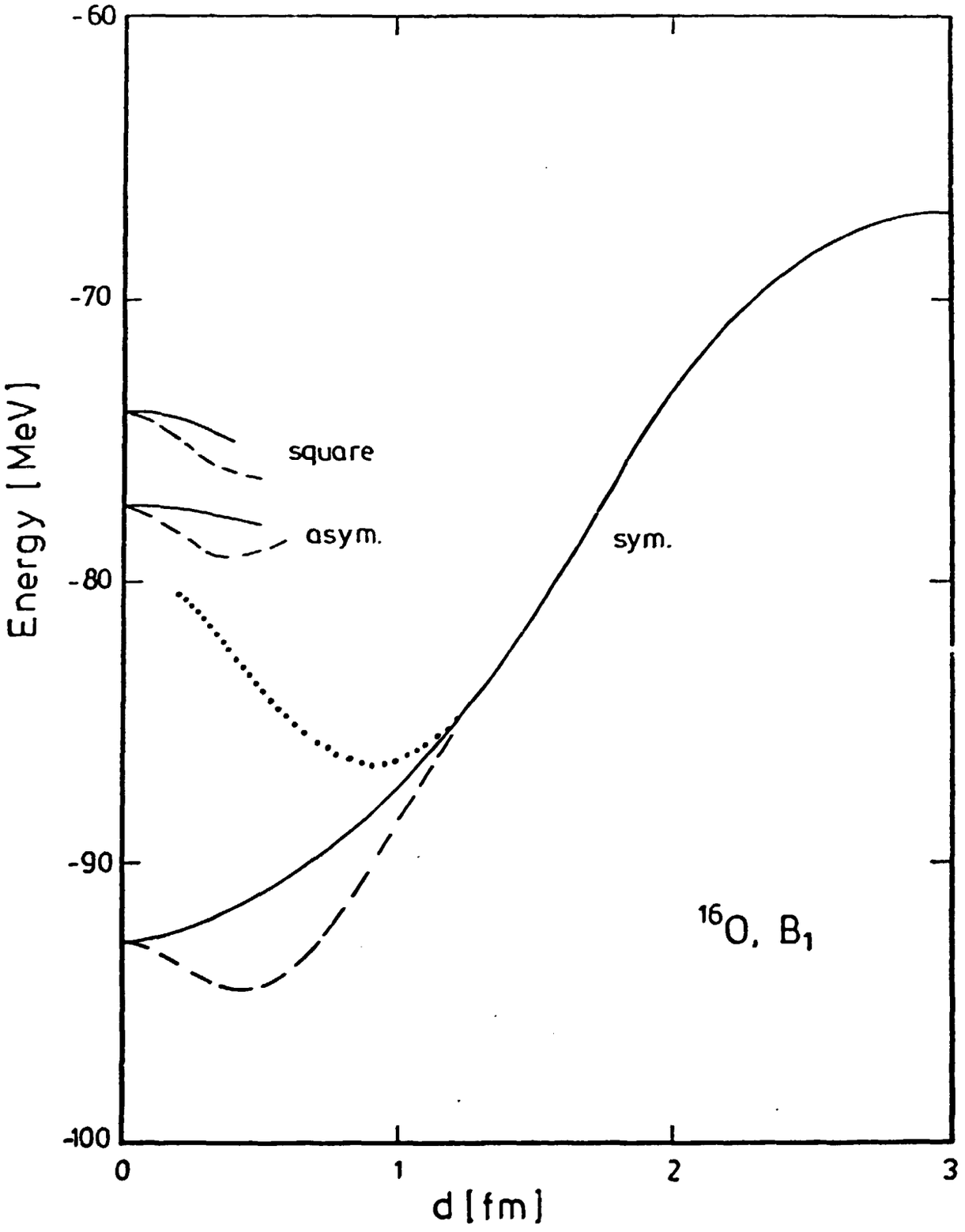

Fig. 2

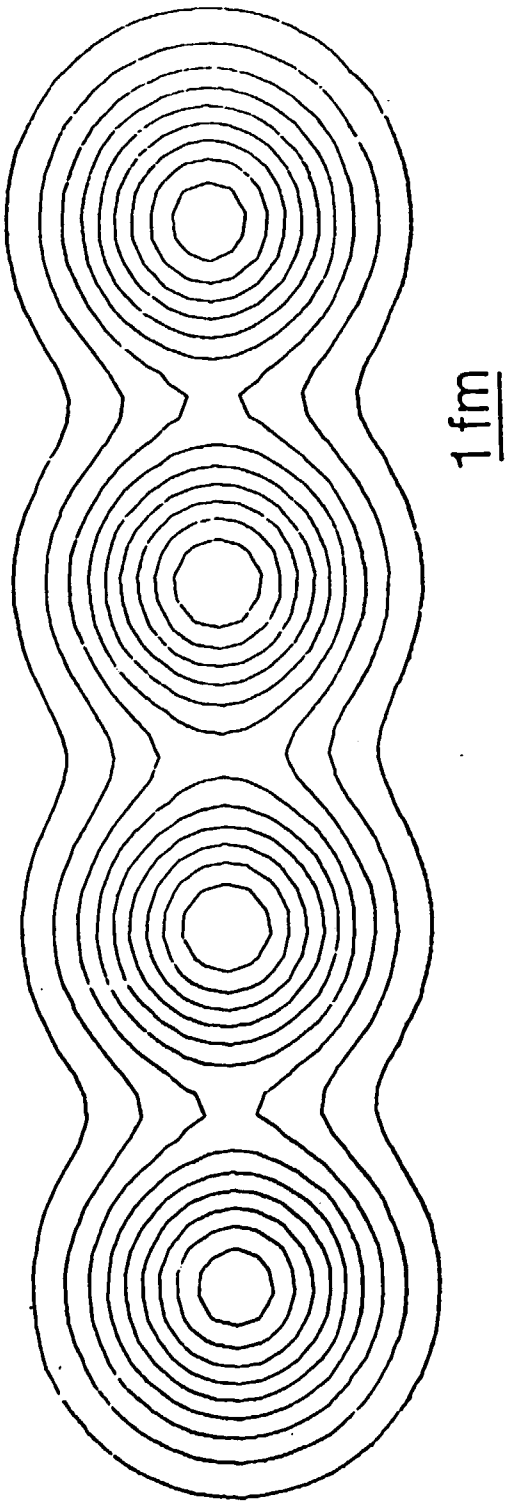

Fig. 3

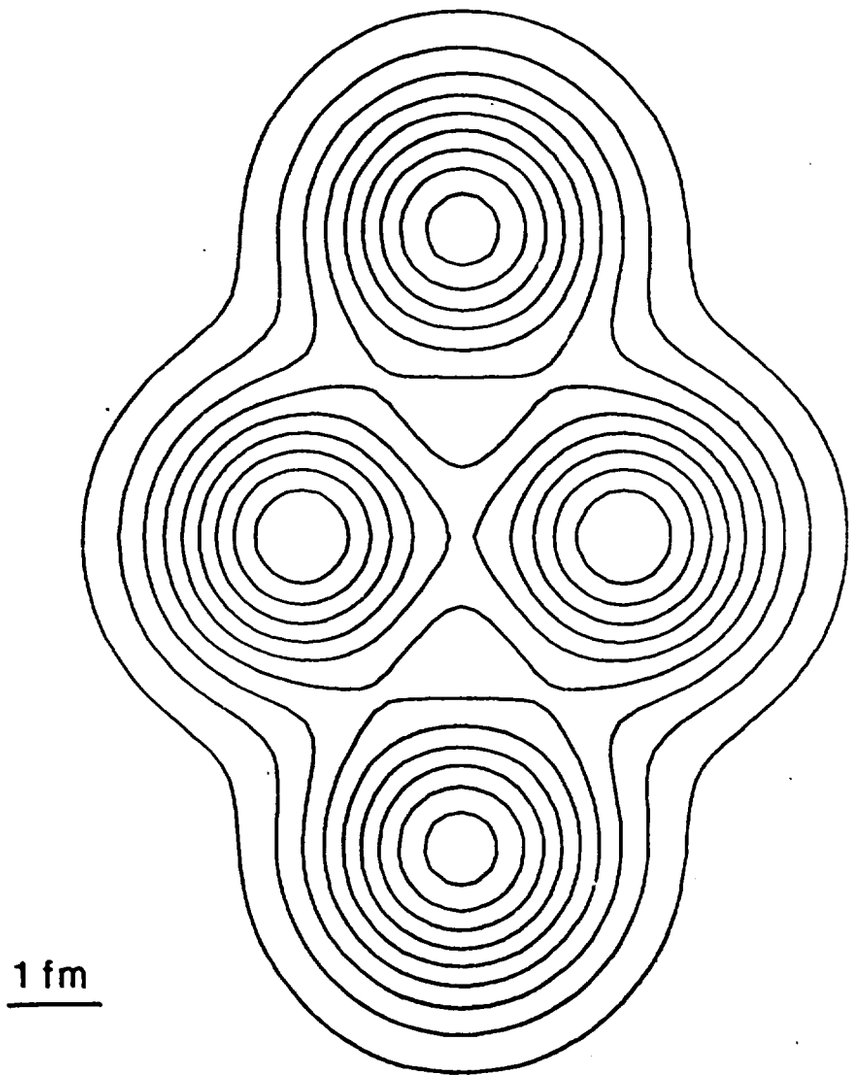

Fig. 4a

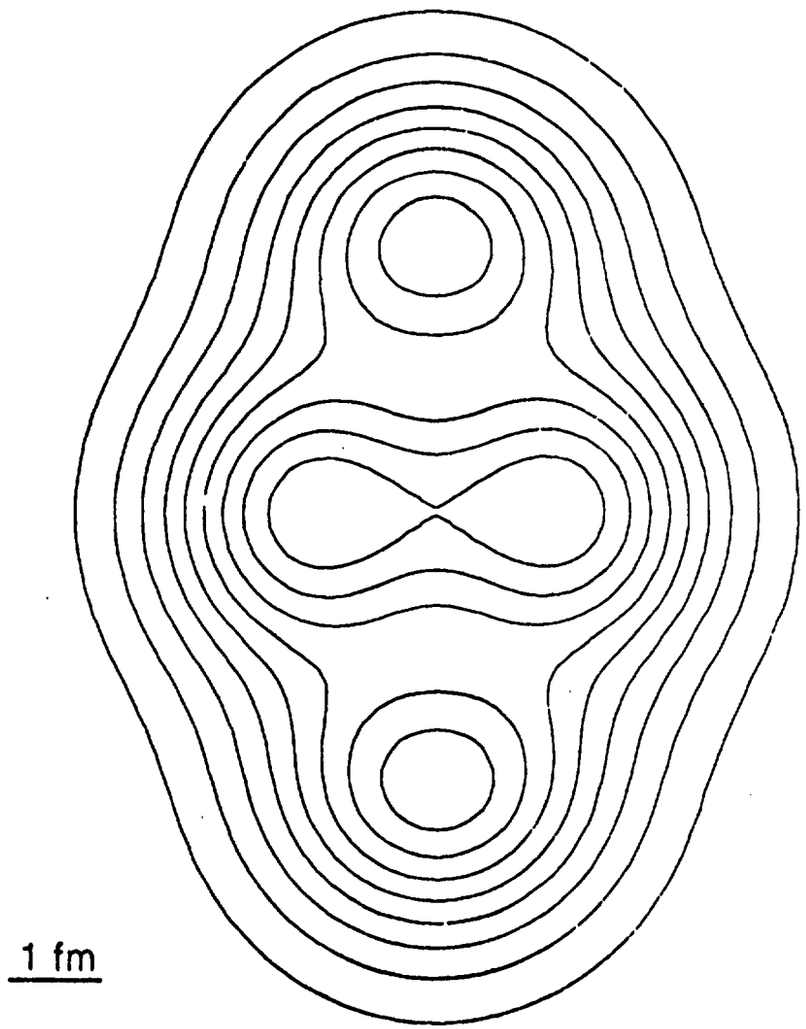

Fig. 4b

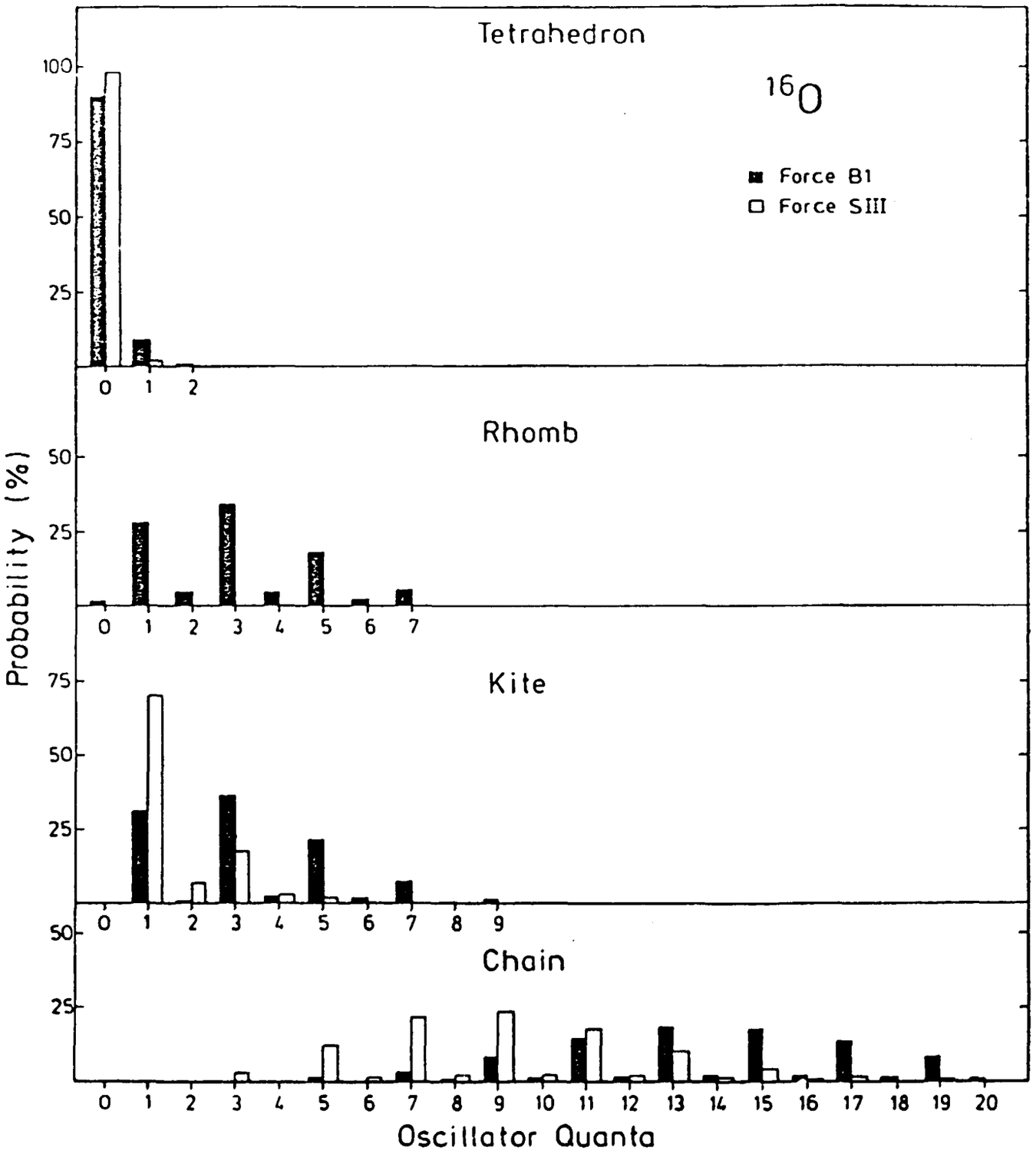
Tetrahedron
^{16}O
Force B1
Force SIII
Rhomb
Kite
Chain
Probability (%)
Oscillator Quanta

Fig. 5

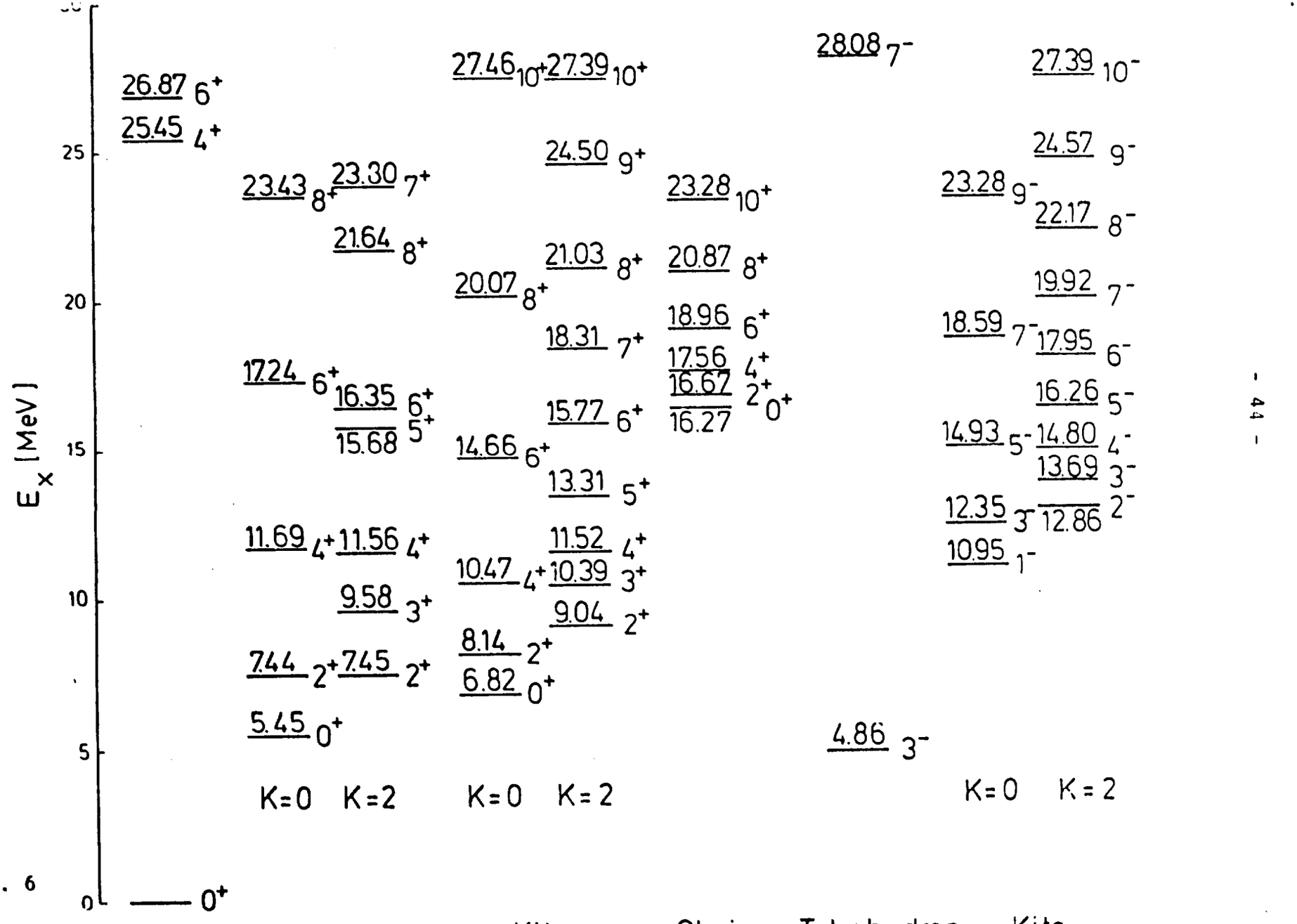
E_x [MeV]
0
5
10
15
20
25
26.87 6+
25.45 4+
23.43 8+
23.30 7+
21.64 8+
17.24 6+
16.35 6+
15.68 5+
11.69 4+
11.56 4+
9.58 3+
7.44 2+
7.45 2+
5.45 0+
0+
K=0 K=2
Tetrahedron
Rhomb
27.46 10+
27.39 10+
24.50 9+
21.03 8+
20.07 8+
18.31 7+
15.77 6+
14.66 6+
13.31 5+
11.52 4+
10.47 4+
10.39 3+
9.04 2+
8.14 2+
6.82 0+
K=0 K=2
Kite
23.28 10+
20.87 8+
18.96 6+
17.56 4+
16.67 2+
16.27 0+
Chain
28.08 7-
27.39 10-
24.57 9-
23.28 9-
22.17 8-
19.92 7-
18.59 7-
17.95 6-
16.26 5-
14.93 5-
14.80 4-
13.69 3-
12.86 2-
12.35 3-
10.95 1-
4.86 3-
K=0 K=2
Tetrahedron
Kite

Fig. 6

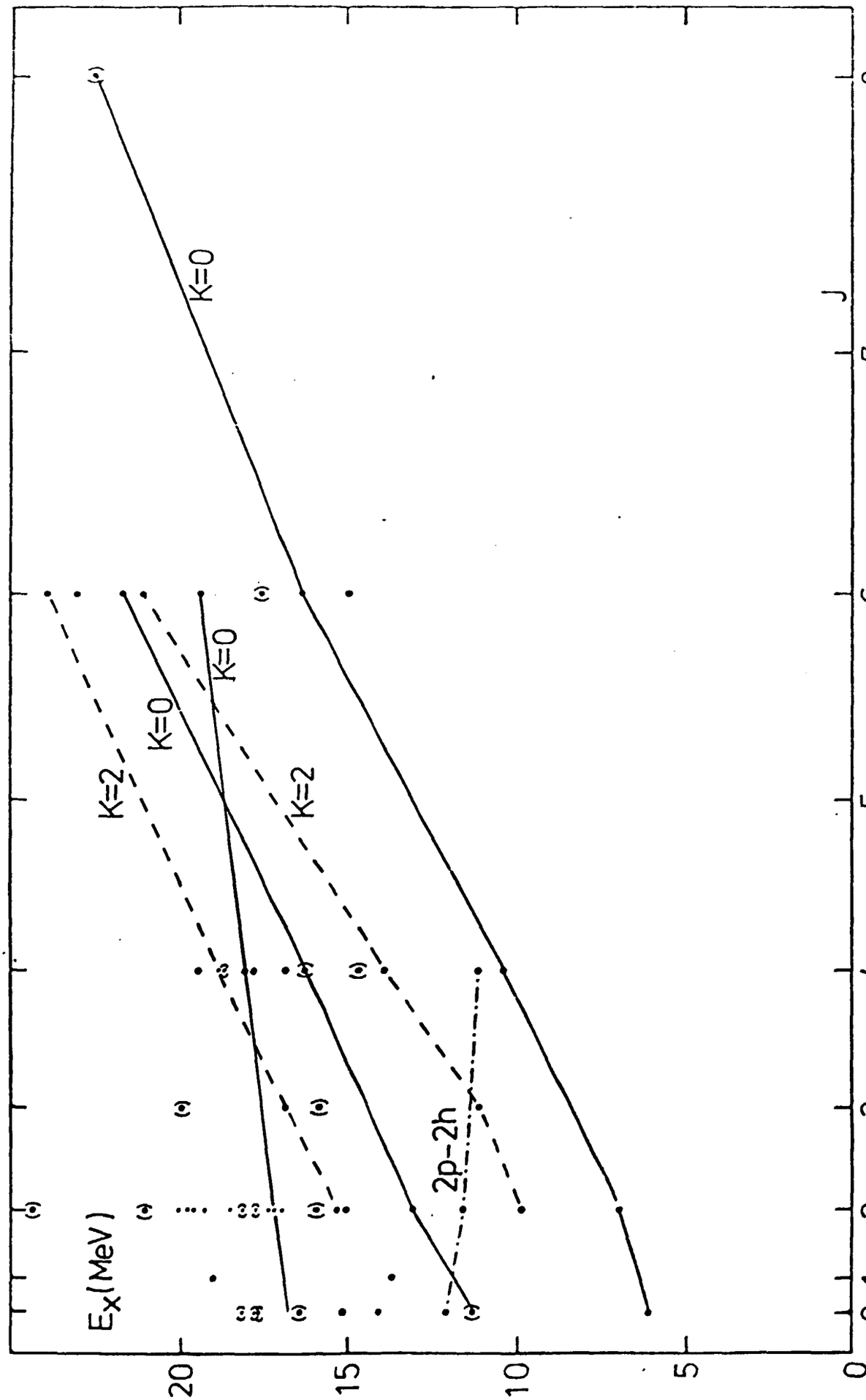

Fig. 7